Annual Report: Year 2

Grant DEFG5206NA2621

Thermoelasticity of SSP Materials: An Integrated Ultrasonic and X-radiation Study

Annual Report for Activities Supported by

DoE/NNSA Grant DEFG5206NA2621

July 2008

Baosheng Li (PI)

Stony Brook University

Donald Isaak (Co-PI)

University of California at Los Angels

Yusheng Zhao (Co-PI)

LANSCE, Los Alamos National Lab

Table of Content

1. Project Objectives

Thermoelastic properties of materials under high pressures P and high temperatures T are of great importance to weapon physics studies. Knowledge about the elastic moduli, equations of state (EOS), and phase stability at high P-T conditions are required when performing computational modeling under the Stockpile Stewardship Programs (SSP). Specifically, accurate information about the pressure derivative of thermal expansion $(\partial\alpha/\partial P)_T$, temperature derivative of bulk modulus $(\partial K/\partial T)_P$, and the Grüneisen parameter γ as a convolution function $\gamma(P,T)$ are necessary to extrapolate existing laboratory data to extreme conditions experienced in a nuclear device. Our recent development of *simultaneous* ultrasonic interferometry and synchrotron X-ray diffraction/radiography at high *P and T* provides a unique means to determine acoustic elasticity and thermoelastic EOS for metals, ceramics, and minerals in crystalline, amorphous, and melting phases. More over, the combined analysis of the acoustic and X-ray diffraction data warrants the accuracy and self-consistency of the derived properties along with a direct measurement of absolute pressure. This project will focus on a comprehensive study of the thermoelastic properties of the SSP materials in terms of sound velocity and P-V-T equation of state. In addition to providing important thermoelasticity data, the success of this project also helps the future integration of ultrasonic interferometry with neutron diffraction/radiography which is currently under development at the Los Alamos Neutron Science Center (LANSCE) for the SSP research of high-Z actinides by taking the advantages of the high penetration and high Q $(4\pi/\lambda)$ of the neutrons.

2. Overview of Project Progress: Year 2

It has been a very productive year for accomplishing the tasks outlined in the original proposal. Quite a few crystalline materials [tantalum (Ta), molybdenum (Mo), cerium (Ce) beryllium (Be)] and amorphous materials [zirconium tungstate (ZrW2O8), SiO2, and germanium diselenide ($GeSe_2$) glasses] have been assessed at high pressures up to 12 GPa and acoustic velocities and densities have been obtained simultaneously using our unique technique. Major activities include sample preparation, high pressure cell assembly testing, and conducting ultrasonic and X-ray diffraction measurements at BNL as well as resonance ultrasonic spectroscopy (RUS) measurements at UCLA on appropriate samples. Sample preparations for Ce and Be were made at Los Alamos National Lab for which special grades and specialized machining of the sample are required. Pilot experiments for optimizing high pressure cell assemblies were conducted using the 1000-ton multi-anvil press (USCA-1000) in the High Pressure Lab at Stony Brook, and simultaneous ultrasonic and X-ray diffraction experiments were conducted using the DDIA apparatus installed at X17B2 of NSLS at BNL. New data analysis protocols have been developed for deriving density of amorphous materials at high pressure and therefore its equation of state. Following on previous years effort, attempts have been made to derive single crystal elastic constants based on the current measurements on polycrystalline samples at high pressure in conjunction with previous data as well as the current RUS measurements at ambient conditions. Single crystal elastic constants of Tantalum have been measured using RUS techniques at room pressure and high

temperature.

Educational and training opportunities have been provided for postdoctoral associate researchers, Drs. Wei Liu (project leader for Mo, and ZrW_2O_8 and SiO_2 glass) and Qiong Liu (Ta project leader) and graduate students Mr. Matthew Whitaker (Project Ce and FeSi) and Sytle Antao (GeSe2 glass project). A total of 6 undergraduate students (2 summer students at Stony Brook University, and 4 undergraduates from Azusa Pacific University) participated in the experiments at various stages and benefited from the discussions about the science and research work conducted by our collaborators of the current project at DoE national labs.

3. Major Findings

3.1 Sound Velocity and Elastic Moduli of Tantalum at High Pressure

Thermoelastic properties of Tantalum have been of long scientific interests for its materials physics and applications. Behavior of Tantalum at high pressure have been studied using both from experimental [5] and theoretical approaches [6] up to its melting temperatures [5, 7-10], at ambient conditions, this transition metal crystallize in body-cenered cubic (bcc) structure with a lattice parameter of a=3.30 angstrom, and the bcc structure is stable to grater than 10 Mbar. Equation of state results for the 298K isotherm have been derived from various high-pressure experiments [5, 9, 11-13] and theoretical calculations[6]. The reported results for the bulk modulus (K_0), however, are still scattered from 188 to 231 GPa, and the associated pressure derivative, K_0', spreads from 2.7 to 4.3, which is not precise enough for predictive modeling of stewardship stockpile under extreme conditions. Prior to the current study, the pressure derivatives ($\partial Cij/\partial P$, and $\partial K/\partial P$, $\partial G/\partial P$) have been accessed by acoustic measurement to a maximum pressure of 0.5 GPa [4], the results are in agreement with shockwave data reduced to 300K isothermal conditions [5, 9, 11-13]. However, some theoretical calculations and static compressions have produced results noticablely different from previous ultrasonic and shock wave measurements. The discrepancies appears to be too large to be reconciled by the uncertainties resulting from different pressure calibrations used in various experimental studies.

In this study, we use a combined ultrasonic interferometry and X-ray diffraction together with synchrotron x-radiographic imaging which allows for not only obtaining P-V-T equation of state and acoustic velocity measurements, but also for direct determination of pressure on the sample. Moreover, the current measurement is conducted at extended pressure range which is about 24 times of the previous ultrasonic measurements on Ta and Mo. The X-ray imaging provides direct and precise (0.2-0.4% in precision) monitoring of the specimen length at high pressure, enabling precise ultrasonic velocity measurements when the deformation of the specimen is beyond its elastic limit (e.g., [14-16] [17-19]). We present here the results of the compressional and shear wave velocities (V_P and V_S), the unit-cell volumes for Ta and Mo to 12 GPa obtained using these state-of-the-art experimental techniques, preliminary results on Ce across the phase transition from g to a, as well as application of the current techniques to amorphous GeSe2 for the study of its elasticity

associated with its densification at high pressure.

Experimental

Polycrystalline Ta sample used in the current study are cylindrical discs with 2.0 mm in diameter. The surfaces were polished and kept parallel within 1 micron (~0.05 degree). The lengths of the two samples after final polishing are 0.584(1) mm and 1.448 mm, respectively.

Compressional (*P*) and shear (*S*) wave velocities at high pressure were measured using a DIA-type, multi-anvil, high pressure apparatus installed on the superconducting wiggler beamline (X17B2) of the National Synchrotron Light Source at the Brookhaven National Laboratory. Details of this experimental set-up and the ultrasonic interferometry have been described elsewhere [20]. Briefly, a mixture of amorphous boron and epoxy resin was used as pressure-transmitting medium. The sample was embedded in a mixture of NaCl and BN powder (10:1 wt%) which provided a pseudo-hydrostatic environment for the sample. A dual-mode $LiNbO_3$ transducer (10° Y-cut) was mounted outside the pressure chamber, which generates and receives both *P* and *S* wave signals simultaneously. To minimize the loss of acoustic energy, all surfaces along the acoustic path, including the ends of the WC cube with transducer mounted, and alumina buffer rod, were also polished and kept parallel within 1 μm. Travel times for *P* and *S* waves were simultaneously measured using the transfer function method with standard deviations of ~0.4 ns for *S* waves and ~0.2 ns for *P* waves [21]. X-ray diffraction patterns for the sample were recorded in the energy dispersive mode using a solid state Ge detector. The incident x-ray beam was collimated to 0.2 mm by 0.1 mm and the diffraction angle was set at 2θ =6.09 degree. Typically, the refined unit-cell volume has a relative standard deviation less than 0.1%. Examples of the raw data recorded are illustrated in Fig. 3.1.1. The high noise to signal ratio and the similarity of the echo pattern between the buffer rod and sample echoes warrant a precise measurement of sample travel time (10^{-4} -10^{-6} precision).

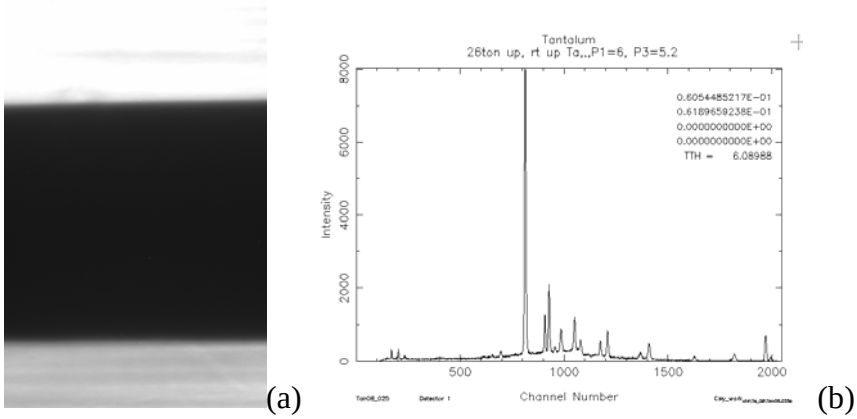

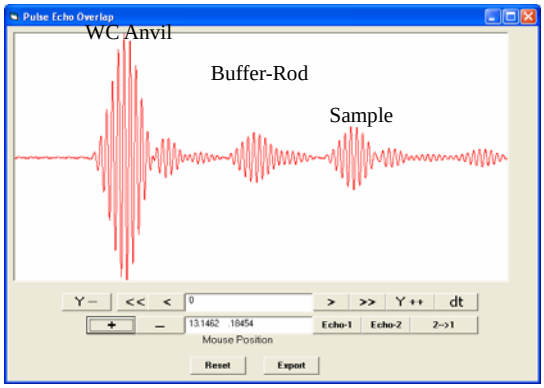

Fig. 3.1.1 (a) Example of (a) sample image (b) X-ray diffraction and (c) acoustic signals recorded in Ta experiment

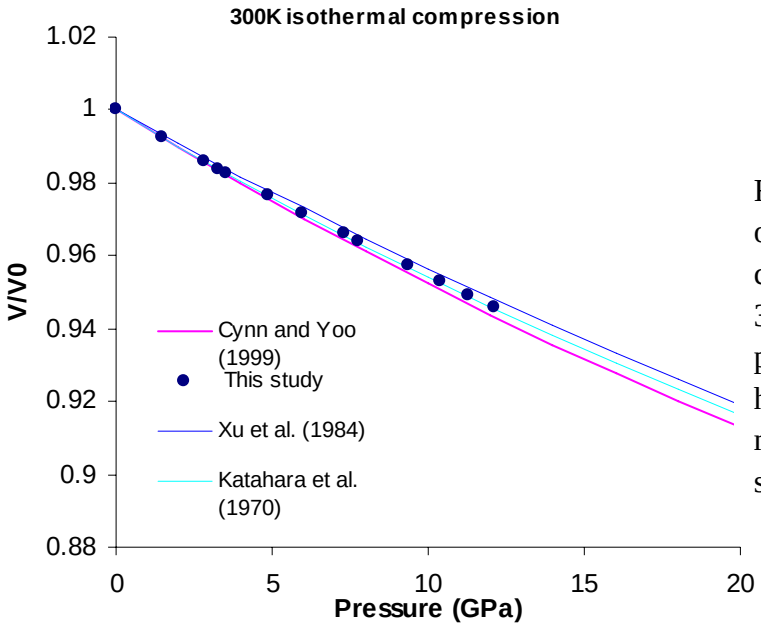

Fig. 3.1.2 Comparison of the isothermal compression curve at 300K with those from previous studies with high and low bulk modulus than the current study.

P and S wave velocities at high pressure

The compression curve of Ta at 300K is compared with three previous studies in Fig. 3.1.2, in which the data of Katahara et al.[4] are obtained from ultrasonic measurements to 0.5 GPa and the other two represent the lowest and highest values of bulk modulus found in X-ray studies. It is clear the current data are in excellent agreement with those of [4], while those from Xu et al.[22] and Cynn and Yoo [23] are higher and lower than the current data, respectively. All other data (not plotted here, refs) essentially fall in the range bracketed by these two studies. When different data listed in Table 3.1.1 are used for pressure determination, a difference of 10% will be resulted.

Figs. 3.1.3 and 3.1.4 show the current results of V_P and V_S at room temperature as a function of pressure and density, respectively. Both V_P and V_S increase monotonically with increasing pressure up to 12 GPa, with pressure derivatives of dV_P/dP =0.031 km/s GPa^{-1} and dV_S/dP=0.016 km/s GPa^{-1}, respectively. As shown in the figure, the data from two experiments, Tan_08 and Tan_10 with maximum pressure up to 6.6 and 12 GPa respectively, are essentially indistinguishable. To obtain the zero–pressure adiabatic bulk and shear moduli as well as their respective pressure derivatives, the velocity and density data in Fig. 3.1.4 are be fitted to the finite strain equations (1) and (2) (Davis and Dziewonski, 1975),

$$\rho V_P^2=(1-2\varepsilon)^{5/2}(L1+L2\varepsilon) \qquad (1)$$

$$\rho V_S^2=(1-2\varepsilon)^{5/2}(M1+M2\varepsilon) \qquad (2)$$

in which $M1= G_0$, $M2=5G_0-3K_{S0}G_0'$, $L1=K_{S0}+4G_0/3$, and $L2= 5L1-3K_{S0}(K_{S0}'+4G_0'/3)$. The strain ε is defined as $\varepsilon=[1-(V_0/V)^{2/3}]/2$. The fitted coefficients, $L1$, $L2$, $M1$, and $M2$ are used for the calculation of the zero-pressure adiabatic bulk and shear moduli (K_{S0} and G_0) as well as their pressure derivatives (K_{S0}' and G_0'), yielding K_{S0}=197.8 (10) GPa, G_0=68.8 (4) GPa,

K_{S0}'=3.78 (2), G_0'=1.3 (1), the RMS (root mean squares) misfits for *Vp* and *Vs* are 0.011 and 0.012 km/s respectively (see Fig. 3.1.5).

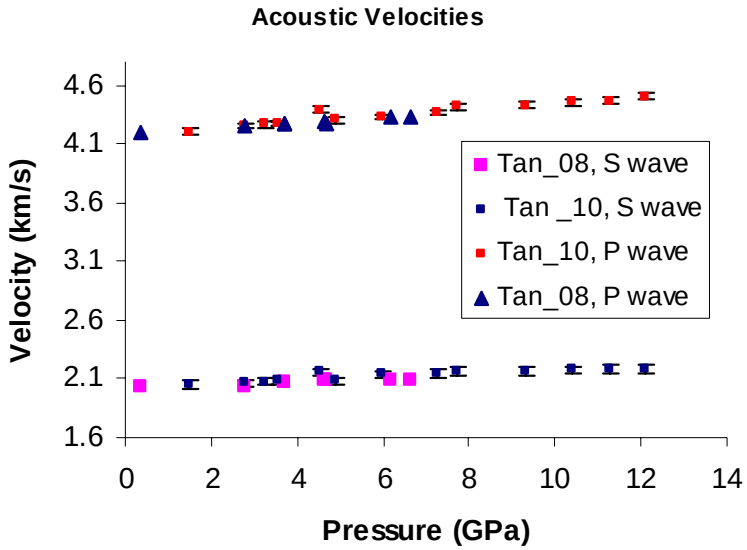

Fig. 3.1.3 *P* and *S* wave velocities of Ta as a function of pressure at ambient temperature. Errors indicated are two standard deviations

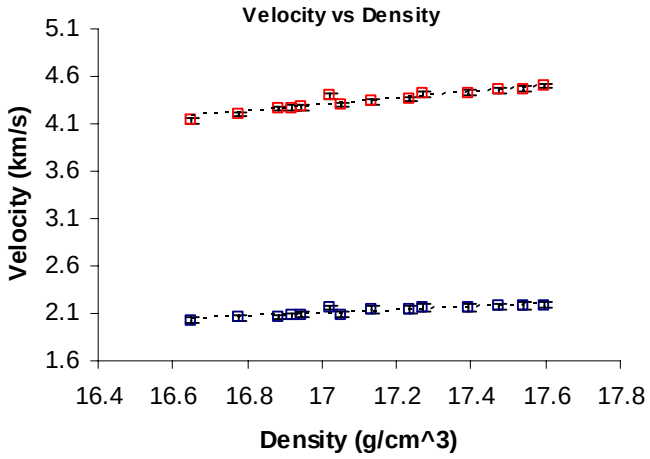

Fig. 3.1.4 Acoustic velocities as a function of density, showing the linear relationship between P (S) wave velocities and density.

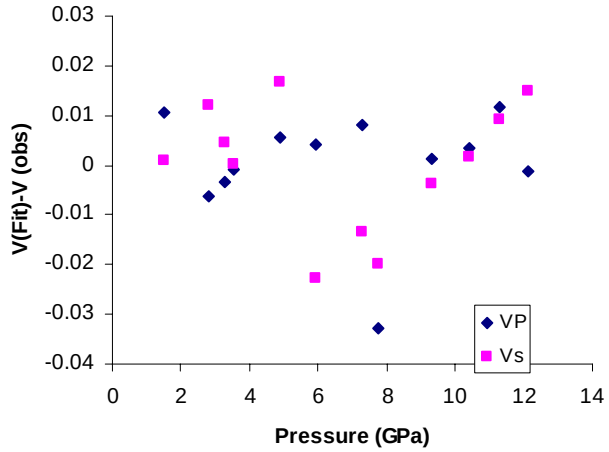

Fig. 3.1.5 Differences between fitted (Vfit) and observed (Vobs) velocities for data collected in run Tan_10.

Table 3.1.1. Comparison of elastic parameters for Ta at ambient temperature.

Method	K_0 (GPa)	K'	G_0 (GPa)	G'	$Pmax$ (GPa)	Reference
Ultrasonic+X-ray	197.8(9)	3.76(1)	68.8(4)	1.3(1)	12	This study
Ultrasonics[a]	195.9	3.79	68.8	1.01	0.5	Katahara et al. (1976)
Ultrasonic[b]	190-196	-				Previous works
Volumetric[b]	206	2.76				Vaida and Kennedy (1970)[b]
Shockwave[a]	195.5(3)	3.60(1)				McQueen et al. (1970)[b]
Calculation	190-209	3.4-4.3			250	Boettger (2001)
Calculations	203	3.71[d]	77.5			Söderlind and John (1998)
Calculations	188	3.95[e]	55	1.1[e]		Gulseren and Cohen (2004)
X-ray	194.7(48)	3.4(1)			174	Cynn and Yoo (1999)
X-ray[b]	231(4)	2.5(20)			80	Xu et al. (1984)[b]
X-ray	194(7)	3.8			8.7	Ming and Manghnani (1978)
X-ray	207.6(15)	2.85(10)			69	

a, VRH from single crystal; b: Data referenced by Cynn and Yoo [23], see references therein. . d: Estimated from a linear fit to 45 GPa and 0.5 GPa data. e: Estimated from a linear fit to data at 7.56 and -0.76 GPa.

In comparison with previous results (Table 3.1.1), the current K_{S0} is in good agreement with the values of the adiabatic bulk modulus K_{S0}=196GPa from ultrasonic and the reduced shock wave data. As indicated in [24], ambiguities in pressure determinations may cause the previous ultrasonic data to vary from 196 to 199 GPa, which is considered within the uncertainties of the current result. The pressure derivative of the bulk modulus K_{S0}' (3.76) obtained from the present study is essentially identical to the low pressure ultrasonic measurement result (K_{S0}'=3.79) within mutual uncertainties. The same conclusion can be drawn for the shear modulus, but the pressure derivatives of the shear modulus are marginally in agreement within mutual uncertainties, with G_0' from Katahara et al. (1970) [4] is 22% lower than the current result. More comparisons with other X-ray studies and theoretical calculations can be found in Table 3.1.1[22, 25-28]. We should note that the apparent discrepancies in the bulk modulus and its pressure derivative might be related to the trade-off between the values of K_{T0} and K_{T0}' in fitting the pressure-volume data to equation of state.

3.1.4 Debye Temperature and Grüneisen Parameter

In addition to the elastic moduli presented above, the data obtained from the current study also allow us to calculate the acoustic Debye temperature Θac obtained using the following relationship,

$$\Theta_{ac} = \frac{h}{k}\left(\frac{3N}{4\pi}\right)^{\frac{1}{3}}\left(\frac{\rho}{M/p}\right)^{\frac{1}{3}}\left(\frac{2}{3v_s^3}+\frac{1}{3v_p^3}\right)^{-\frac{1}{3}} \quad (3)$$

where M is the molecular mass; p is the number of atoms in the molecular formula; and k, h and N are Boltzmann's constant, Plank's constant, and Avogadro's number, v_p and v_s are the compressional and shear velocities, respectively. The Grüneisen parameter can be obtained from the elastic moduli and their pressure derivatives, which can be used to calculate the shockwave compression along Huogoniot. Other properties, such as Poisson's ratio σ, Yong's modulus E, and shear strength (using Steinberg-Guinan strength model, $Y=Y0f(\varepsilon_P)G(P,T)/G_0$) can all be assessed. This work is still ongoing.

3.2 Single Crystal Elastic Constants of Tantalum

a. RUS measurements at high temperature

RUS has been commonly used to make accurate determinations of the elastic constants at ambient and high temperatures. Novel elastic properties of Ta are of fundamental importance for understanding highly correlated electronic systems. During this fiscal year, we continued our efforts in obtaining single crystal elastic constants using RUS methods. Raw data have been collected on a single-crystal Ta specimen (5.208 cm × 5.070 cm × 4.958 cm) which was cut and polished into the shape of a rectangular parallelepiped with faces parallel to the three mutually orthogonal (100) planes. We carefully measured and identified the lowest 40 resonant modes at room temperature using a specimen-to-transducer holding force equal to the weight of only 0.5 g. The adiabatic bulk modulus (K_S) and two shear moduli [C_{44} and $C_S = (1/2)(C_{11}-C_{12})$] determined from these resonant frequencies are: K_S = 191.6(9) GPa, C_{44} = 82.3(1) GPa, and C_S = 52.5(1) GPa. We note that the shear modulus from RUS measurement (G (VRH) = 68.7GPa) is in excellent agreement with the ultrasonic measurements on polycrystalline sample, although the bulk modulus is about 3% lower than the ultrasonic interferometry measurement.

As reported earlier, we heated the tantalum from 300 K to 850 K in increments of 50 K to obtain spectra, and thus elastic properties, at elevated temperature. A sample of the spectra at three temperatures is shown in Figure 3.2.1. The elastic constants of Ta were obtained using 30 of the 40 lowest modal frequencies in the high-temperature analysis. The temperature dependence of elasticity determined in our analysis is shown in Figures 3(a)-(c). For comparison, results from two previous determination of Ta elasticity, both using a pulse-echo technique, are also shown.

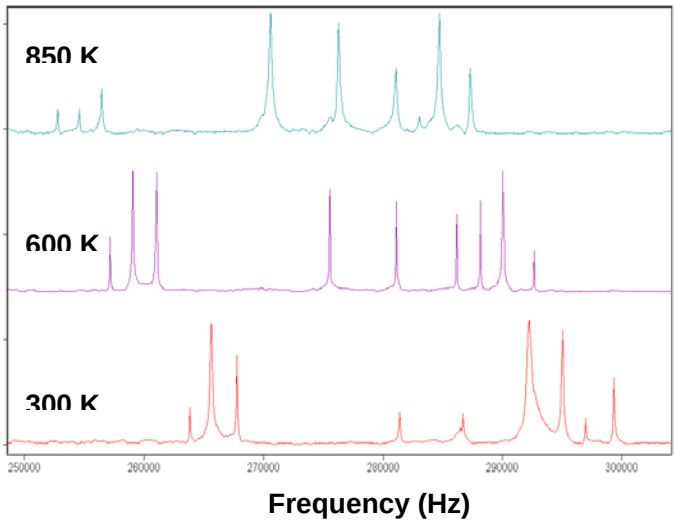

Figure 3.2.1 Sample of spectra of single-crystal specimen of tantalum at 300 K, 600 K, and 850 K showing temperature dependences of eleven modal frequencies. The 'y-axis' indicates vibration amplitude in arbitrary units.

on thin wires of Ta from room temperature up to nearly 900 K. However, our data are consistent with the clear, even if unpronounced, nonlinearity of $C_{44}(T)$ seen in data from both ref [29] and [30]. Walker and Bujard [29] discuss anomalous nonlinearity of $C_{44}(T)$ in terms of band structure, i.e., features of the Fermi surface, that occur in some 4*d* and 5*d* transition metals. They note this effect is very pronounced in niobium and vanadium, to the point of producing a minimum in C_{44}, at which point C_{44} becomes larger with increasing temperature. The ref [29] to higher temperature (the melting point of Ta), however, does not identify such a drastic effect in C_{44} for tantalum. During this year, we have attempted to buffer tantalum with an inert gas (Argon) in order to expend the measurements to higher temperatures well in excess of 850 K. However, even with a steady flow of highest purity Ar gas, the specimen showed clear signs of degradation on its surface when reaching 900 K. Hence, we deem our results obtained up to 850 K are reliable. We are now in the process of trying the apparatus with a vacuum pull and expect soon to find out whether its feasibility of acquiring data at much higher temperatures than 850 K.

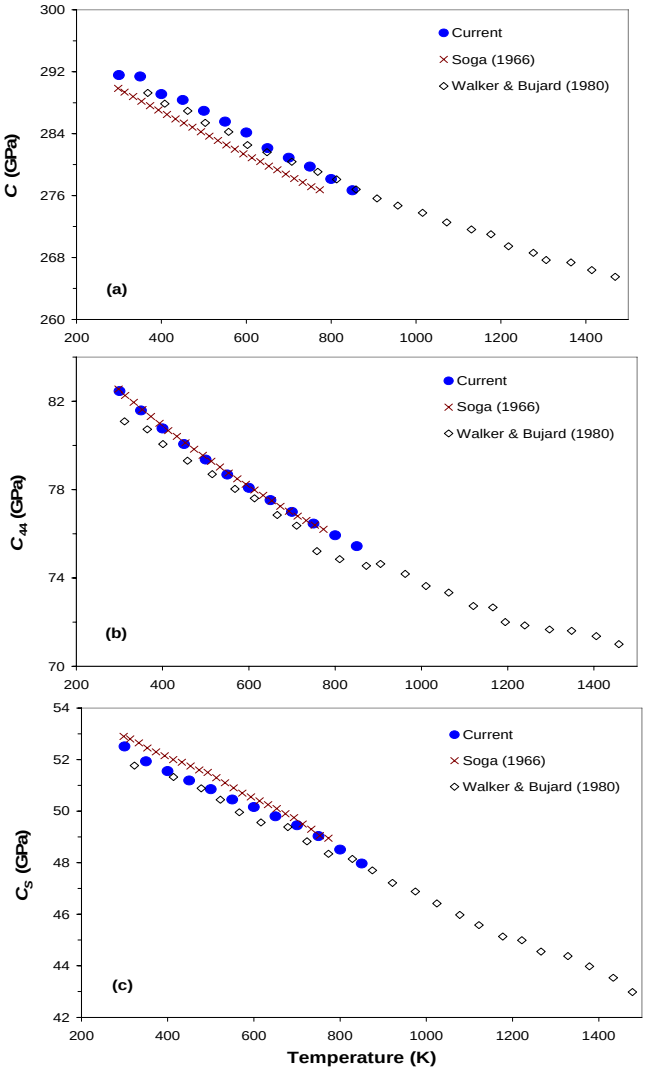

Figure 3.2.2 (a)-(c) Results of current determination of elastic moduli of Ta from 300 to 850 K using RUS. Comparison is with earlier results from pulse echo studies. In (a) and (c), C and C_S are $(1/2)(C_{11} + C_{12} + 2C_{44})$ and $(1/2)(C_{11}-C_{12})$, respectively.

b Elastic Constants of Tantalum at High Pressures

Following the approaches established in our last year's report, we made the attempt to derive the elastic constants C11, C12, C44 from the measured density, Vp and Vs using polycrystalline sample. This is done by a least squares fit to the measured velocities following a procedures modified from [31], in which, according to 3rd order finite strain theory, the elastic constants at high pressure can be prescribed by the values of the elastic constants and their pressure derivatives at ambient pressure. The expressions for pressure, bulk modulus and shear modulus are given in eqs. (4)-(7).

$$P = (1+2f)^{\frac{5}{2}}[3K_0 f + (3K_0K_0'-5K_0)f^2] \quad (4)$$

$$K = (1+2f)^{\frac{5}{2}}[K_0 + (3K_0K_0'-5K_0)f + \frac{27}{2}(K_0K_0'-4K_0)f^2] \quad (5)$$

$$G = (1+2f)^{\frac{5}{2}}[G_0 + (3K_0G_0'-5G_0)f + (6K_0G_0'-24K_0-14G_0+\frac{9}{2}K_0K_0')f^2] \quad (6)$$

$$f = \frac{1}{2}[(\frac{\rho}{\rho_0})^{\frac{2}{3}} - 1] \quad (7)$$

If the f^2 terms are left out, then these equations are equivalent to Eqs. (1) and (2) except they are expressed in terms of K and G instead of velocities. For cubic material, K and G are related to the single crystal elastic constants by $K=(C11+2C12)/3$, and $G=(G_V+G_R)/2$ (Voigt-Reuss-Hill average) with $G_V=(C11-C12+3C44)/5$ and $G_R=5/(2/C'+3/C44)$. With constraints on the elastic constants at ambient conditions from ref [26] and the pressure derivatives K' and G' in Table 3.1.1, the elastic constants at high pressures are derived by minimizing the difference between the calculated and observed velocities V_P and V_S, and the results are shown in Fig. 3.2.3. For comparison, the results extrapolated from previous ultrasonic measurement in [4] are also included, together with those from theoretical studies [1] and [3]. The current C11, C12 and C44 are in close agreement with those extrapolated from low pressure measurements [4], the differences at 12 GPa between the current C11, C12 and C44 and those extrapolated ones are about 3-4% which is considered within the precision of the above inversion procedures. This approach, although pending to be tested for other cubic materials, presents a novel method for estimating single crystal elastic constants at high pressures by measuring polycrystalline sample only.

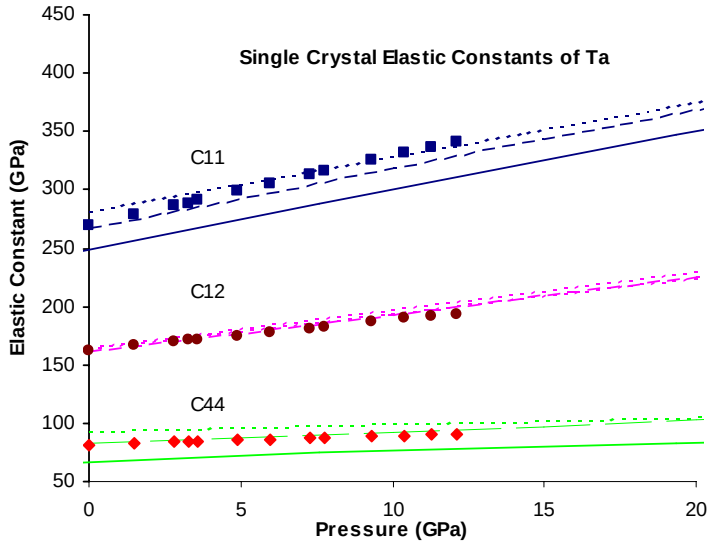

Fig. 3.2. 2 Comparison of elastic constants Cij at high pressure. Symbols- this study; dotted lines: ref [1], solid lines- ref [3], and long dashed lines- ref [4].

3.3 Thermoelastic Properties of Molybdenum

Molybdenum is another refractory metal that has been studied this year. In addition to its various industrial and nuclear applications, molybdenum is also often used as a high-pressure standard in diamond anvil cell experiments [32], and there has been much interest in static equation of state and dynamic behavior of this material [33-35]. Static compressions have been conducted to 272 GPa at ambient temperature, and was found remain in the bcc phase, a transition to a possible hcp (or fcc) phase observed in previous shock wave experiment at 210 Mbar 4100K was not evident which could be hindered by the low temperature in DAC experiment. To relate shock and static data, knowledge of pressure, thermal and strength effects derived from static compression or ultrasonic measurements is often needed.

Previously, single crystals of Mo have been performed up to 0.5 GPa and pressure derivatives of the elastic constants were reported [36]. It is controversial whether the low pressure derivatives of the bulk modulus derived from static compression studies are a reflection of the higher experimental pressure range or just the trade-off between K and K' in Eos fitting. This parameter is important when extrapolating to shock pressures for modeling or reducing shock response along Hugoniot.

Following the procedures described in section 3.1 for Tantalum, we have conducted measurements on Mo using polycrystalline sample. The sample is a cylindrical disk of 2mm in diameter and ~0.8 mm in thickness; it has a bulk density of 9.942 g/cm^3 which is about 97.3% of X-ray density of 9.98 g/cm^3. Information about the impurities is still to be analyzed; we therefore attribute the density deficiency to the total effect of porosity and impurities.

Similar to those described for Tantalum, the Mo sample was pressurized in a 250-ton D-DIA type high pressure apparatus, after reaching peak pressure of ~12 GPa, the sample was heated to a maximum temperature of 1273 K, after which a dense collection of X-ray diffraction, acoustic and X-ray imaging data were made to cover a wide range of P-T space, as showing in Fig. 3.3.1.

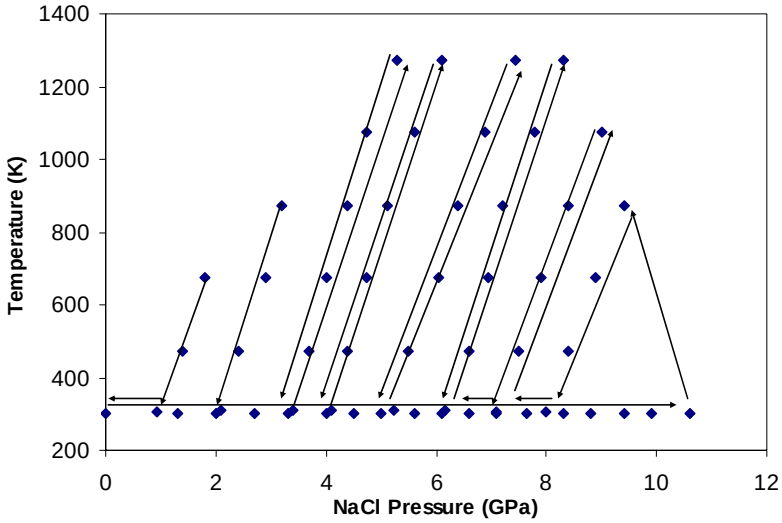

Fig. 3.3.1: Experimental P-T path in Mo experiment. Symbols represent conditions that data were collected. The lines with arrows indicating the path of pressurization /decompression and heating /cooling

From the recorded X-ray diffraction data, the unit cell volumes of Mo were obtained by a least squares refinement. The results are shown in Fig. 3.3.2. We notice that the 300K volumes obtained along cold compression are lower than those measured after the sample was cooled from high temperature by about a constant value of 0.1A^3. This could be related to the different stress state between cold compression and after heating. While this difference is still to be understood and reconciled, we did not use these cold compression data for equation of state analysis. In Fig. 3.3.2, we also plotted the data from Zhao et al. [37] which were obtained in a pressure and temperature range similar to those in the current study. Except those along 1273K isotherms, data from these two studies, represented by solid and open symbols of the same color, are in very good agreement. A preliminary high temperature equation of state analysis using 3rd order Birch-Murnaghan EoS gives dK_T/dT= -0.038(5) GPa/K which is in good agreement with dK_T/dT= -0.034(9) GPa/K obtained by Zhao et al. (2000) when all other parameters are identical. If the adiabatic bulk modulus K_S (262 GPa) and its pressure derivative K_S' (4.73) are constrained using the ultrasonic data while the

thermal expansion is constrained as $\alpha=1.32x10^{-5}+1.26x10^{-8}T$, the temperature derivative dK_T/dT obtained from fitting the current data is -0.035(5) GPa/K. Currently, we are exploring the differences when different equations of state are employed, such as high T Birch-Murnaghan and Vinet EoS. Once these are finalized, a comprehensive study about the Grüneisen parameter, Debye temperature as well as other thermodynamic parameters will follow.

At present, we have fully analyzed the acoustic data at room conditions along cold compression. The velocities at high pressure and ambient temperature are given in Fig. 3.3.3 as a function of density. Applying finite strain fit to these data, we obtained the elastic moduli and their pressure derivatives and the results are compared with previous data in Table. 3.3.1.

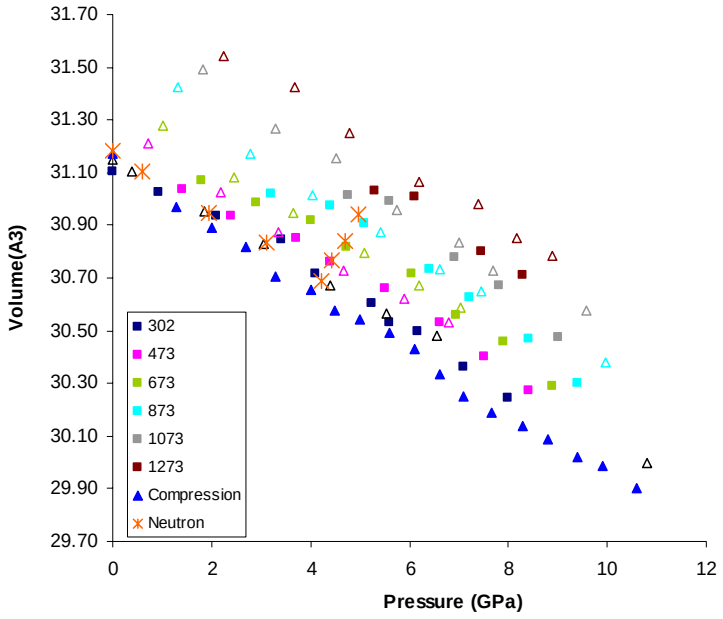

Fig. 3.3.2 Unit cell volumes of Mo observed in the current experiment along different isotherms. Solid symbols: this study; Empty symbols: Zhao et al. (2000); Asterisks: Neutron data from Zhao et al. (2000); Solid and open symbols with the same color are at the same temperature. Temperature labels are in Kelvin.

.

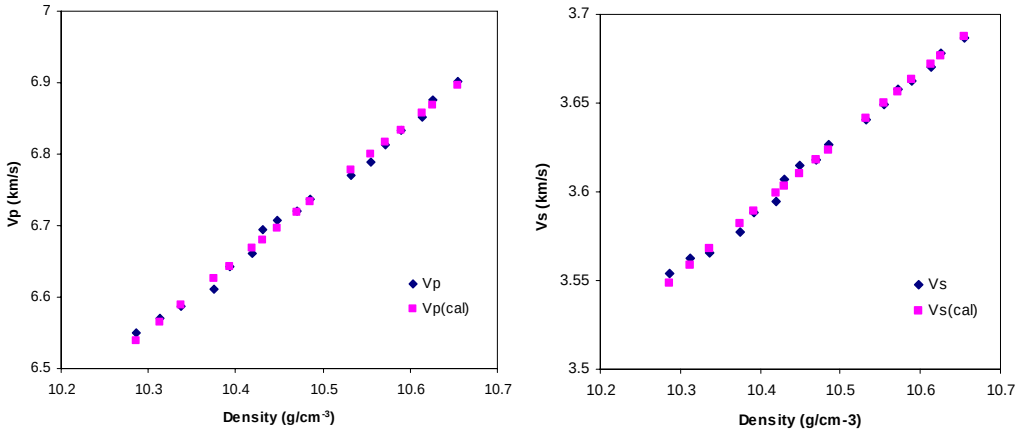

Fig. 3.3.3 P and S wave velocities of Mo as a function of density. Black symbols are observed data and pink symbols are those from finite strain fit using Eqs. (1) and (2).

As seen in the table, the data from different studies are found in agreement within 3% for the bulk and shear moduli at ambient conditions in spite of the experimental pressure range,

and the pressure derivatives are within 10% which is also considered in good agreement if we account for the trade-off between K and K' in equation of state fitting. Of particular interest is the comparison between the current data with those from previous ultrasonic measurements up to 0.5 GPa. As the data analyses stand now, the pressure derivatives obtained from cold compression are higher by 6-10%. We are in the process of analyzing the high temperature velocity data and soon we can find out if the results at ambient temperature after heating agree with the cold compression data.

Table 3.3.1 Comparison of the elastic moduli and their pressure derivatives at ambient temperature*

	$K_{S\ (GPa)}$	G (GPa)	K_S'	G'	K_T (GPa)	K_T'	Notes
Bolef and de Klerk (1962)[38]	268.3	124.6					Single crystal, ultrasonic, 77-500K
Featherston and Neighbours (1963)[39]	261.9	126.7					Single crystal, ultrasonic, 4.2-300K
Dickison and Armstrong (1967)[40]	262	125.8					Single crystal, thin rod resonance, -198-650 ^oC
Davidson and Brotzen (1968)[41]	263.8	126.4					Single crystal, ultrasonic, -190-100 ^oC
Katahara et al.(1979)[36]	262.6	124.4	4.44	1.43			single crystal, ultrasonic, to 0.5 GPa
Carter et al. (1971)					267	3.9	Shock data[a]
Vohra and Ruoff (1990)[42]					262.8	3.95	DAC, to 272 GPa
Zhao et al. (2000)[43]					268 (1)	3.81 (6)	EoS, X-ray, 10 GPa and 1475 K, with shock data
This study	259	126.9	4.73	1.58			Ultrasonic, 3rd FS, to 12 GPa

*: Ultrasonic data are adiabatic values and the X-ray results are isothermal values. a: See Zhao et al. (2000)[43].

3.4 Anomalous Elasticity of Cerium across γ - α Phase Transition

Progresses have also been made on elasticity measurements of cerium (Ce). It is known that this 4f-electron metal undergoes several phase transformations at pressures below 10 GPa (see Fig. 3.4.1) [2, 44-48]. At ambient conditions, Ce is stable in γ-fcc phase, transforming into α-fcc at pressure around 0.7 GPa with a volume collapse of 13-16%. This has been suggested to be an indication of the delocalized 4f electrons in Ce. Much of the debate in the literature has been on the stable phases at pressure range of 5-13 GPa[49-51], where some studies have found that the α-U structure is the stable phase while others suggested the body centered monoclinic α" phase. It has been proposed that the preparation of the sample such as filed versus cut samples, might be important in producing different phases in these experiments at these pressures.

We have acquired four high purity specimens from Los Alamos National Lab, and

conducted measurements at the P-T conditions shown in Fig. 3.4.1. At first the sample was compressed at room temperature to about 9 GPa, during which the phase transition from γ -> α was observed; at around 3.7 GPa, the sample appears to be in the α-U phase (α') and the presence of the α" phase was not evident. Upon heating at ~9 GPa, the α-U phase was transformed back to α phase and high temperature data were collected while the sample was kept as the α phase. The X-ray diffraction pattern of alpha phase at peak P-T conditions is shown in Fig. 3.4.2.

We have finished the preliminary data analysis on the data collected along compression at ambient temperature. The unit cell volume results are shown in Fig. 3.4.3. The results from two experiments (Run_04 and Run _05) are in complete agreement throughout the pressure range of the current study. The volume collapse at the phase transition from γ to α phase is 14.8% which is in excellent agreement with previous X-ray diffraction studies.

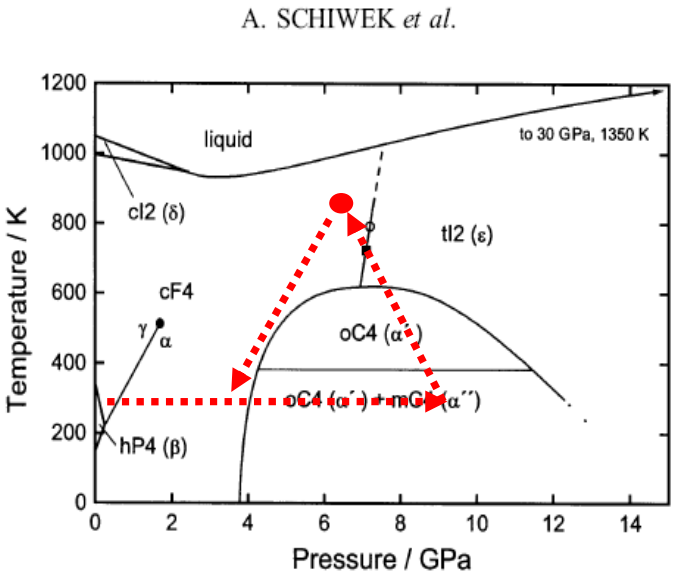

Fig. 3.4.1 P-T path examined in the current experiment (green shaded area) superimposed on the phase diagram of Ce. After Schiwek et al.[2]

More importantly, the acoustic velocities across this phase transition are captured using the techniques described above. These results are shown in Fig. 3.4.4. Although the signals become largely attenuated in this pressure range, our preliminary analysis suggest that both P velocity of γ phase shows a monotonic decrease with increasing pressure up to the transition, while S wave appears to increase slightly and then decease with pressure. It is noted that the S wave signal becomes very weak in the pressure range 0.4-0.7 GPa, making the travel time determination difficult. After the phase transition to α phase, it is clear that the velocities start to increase with pressure, but the compressional wave V_P may undergo softening around 5 GPa while approaching the transition to α' phase, again, the S wave becomes too weak to be measured. We will conduct more experiments to further confirm and expend these results, especially to conditions near the critical point.

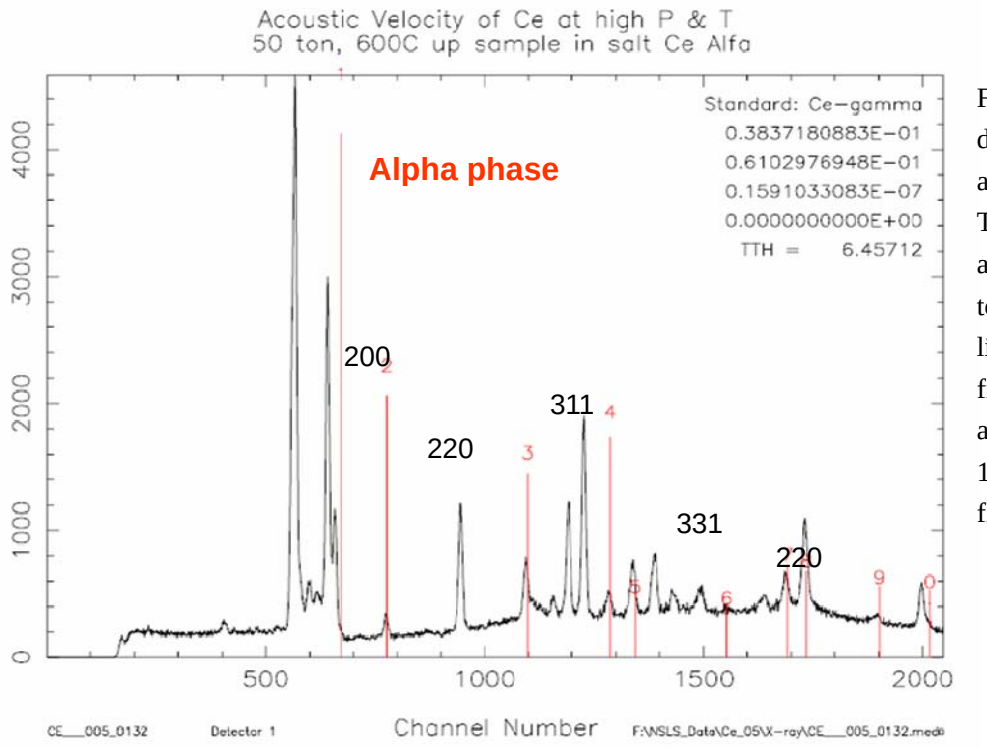

Fig. 3.4.2 X-ray diffraction pattern at ~ 6GPa 873K. The indexed peaks are corresponding to α phase; the red lines mark peaks from NaCl. Peaks around channel 1100 are Pb florescent peaks.

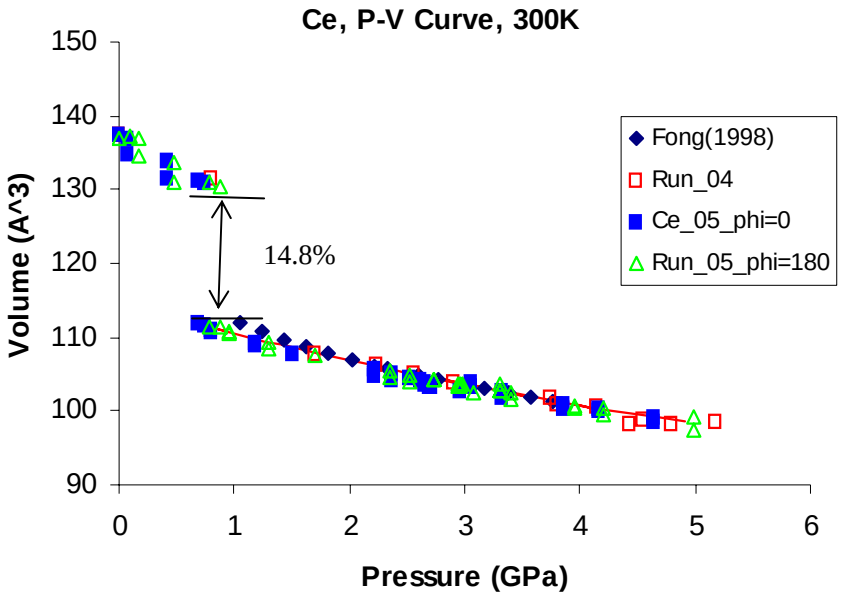

Fig. 3.4.3 Volume of Ce as a function of pressure from X-ray diffraction data. Blue, and Green symbols are from the Run_05 and red squares are from Run _04, black diamonds are from Fong (1998).

From the measured density (calculated from unit cell volume), the elastic bulk and shear moduli K and G are also determined. If is clear that γ-fcc phase of Ce becomes more compressible with increasing pressure up to the transition point, while shear modulus exhibits strengthening to 0.3-0.4 GPa followed by softening when approaching the phase boundary. For α-fcc phase, the behavior of K and G appears to be normal, with a derivative of K' ~ 4

and G' 2.7, respectively. We also compared with the current bulk modulus with previous estimations in Fig. 3.4.6. The general trends observed in previous studies are in close agreement with the current findings, but the data are much more scattered. This year's plan for this material is to optimize the sample size for use with the current cell assembly so that high quality data can be acquired to higher pressures and at high temperatures.

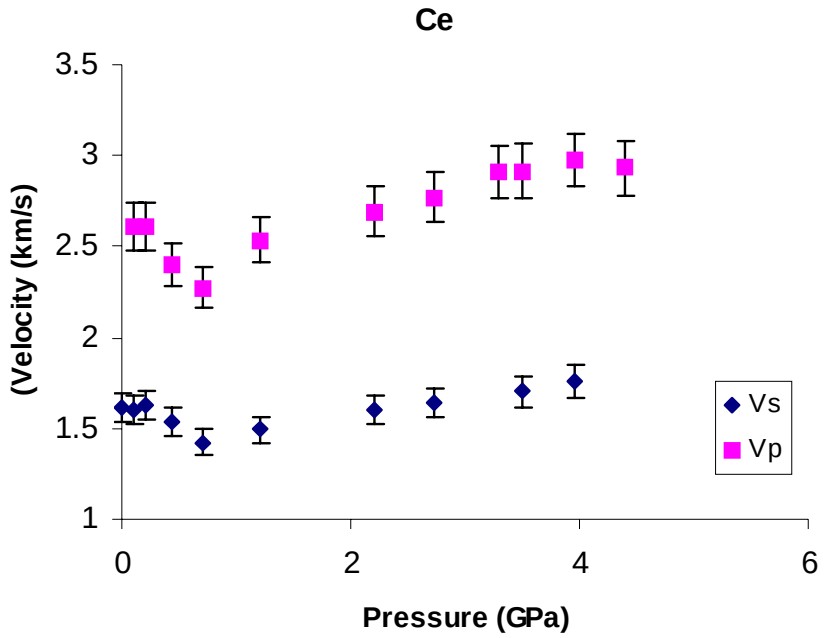

Fig. 3.4.4 P and S wave velocities as a function of pressure for Ce.

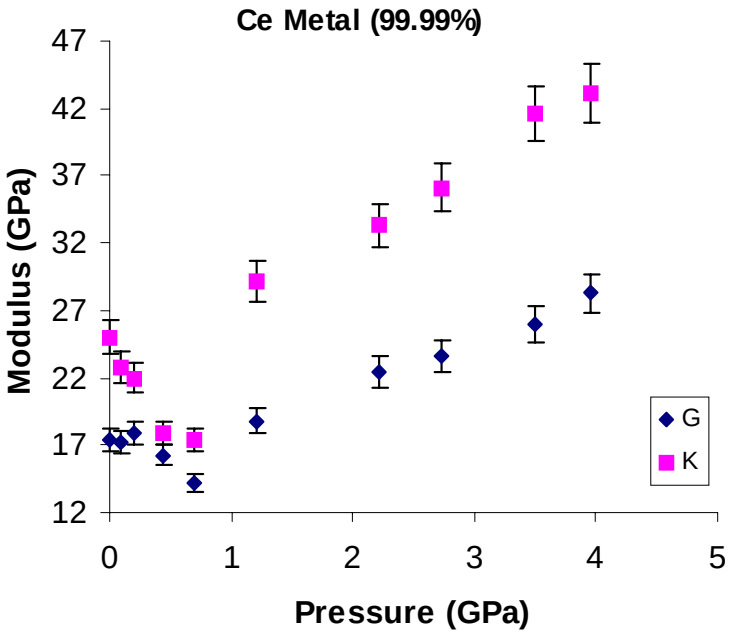

Fig. 3.4.5 Elastic bulk and shear moduli as a function of pressure for Ce.

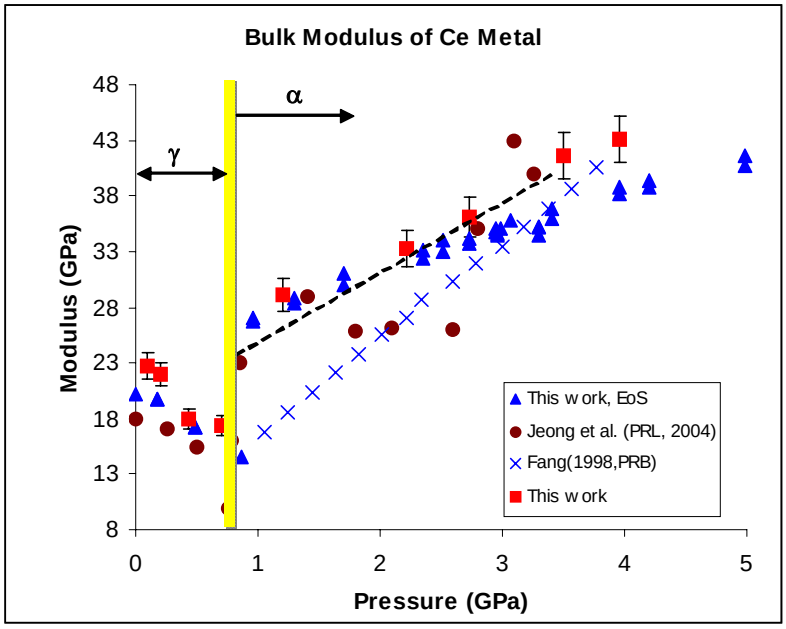

Fig. 3.4.6 Comparison of bulk modulus obtained from the current study and those from previous studies across the phase transition from γ to α phase.

3.5 Velocity and Density Measurements on Amorphous Materials at High Pressure

In the development of techniques for velocity measurements on melts and quenched glass, we conducted a few feasibility tests using amorphous solid to optimize the cell assembly. These include zirconium tungstate, ZrW_2O_8 glass amorphized at pressure recovered at 5 GPa from compressing of crystalline material, SiO_2 glass, and $GeSe_2$ glass. While the data analyses for ZrW_2O_8 and SiO_2 are still ongoing, the velocity data on $GeSe_2$ have been completed and will be highlighted here.

Shear Flexibility of GeSe2 glass at High Pressure

Prior to our velocity measurements, structural information about $GeSe_2$ densification have been acquired from high energy X-ray studies [52, 53]. In this study, acoustic measurements using synchrotron radiation have been performed on glassy GeSe2 up to pressures of 9.6 GPa. During the experiment, we took special precautions in controlling the sample stress state by advancing/ retreating the vertical component of the applied force to the cell assembly so that the sample would not experience plastic deformation. Both P and S wave showed high signal to noise ratio throughout the experiment to ~10 GPa. The results are summarized in Fig. 3.5.1. The minimum observed in the *S*-wave velocity with pressure for GeSe2 glass at 4 GPa is interpreted as a result of competition between these two densification mechanisms. Namely, at low pressure <3 GPa the network becomes more flexible as the connectivity decreases due to the breakup of cross-linking elements. Above 4 GPa the covalently bonded network progressively stiffens as its mean coordination number increases. On depressurization, both velocities decrease irreversibly to ambient pressure due to permanent densification, and no minima is observed in V_S. Isotopic neutron and high-energy x-ray diffraction data on GeSe2 glasses recovered from 10 GPa show that on depressurization

the Ge-Se bond length remains elongated and, although the compacted samples revert back to tetrahedral coordination, they remain highly distorted.

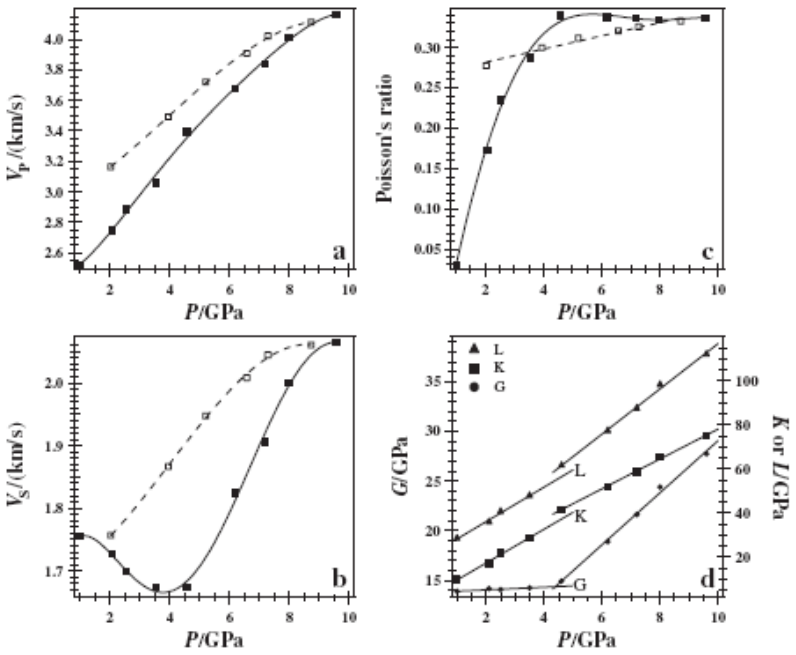

Fig. 3.5.1 Experimentally observed P and S wave velocities, Poisson' ratio and shear modulus as a function of pressure.

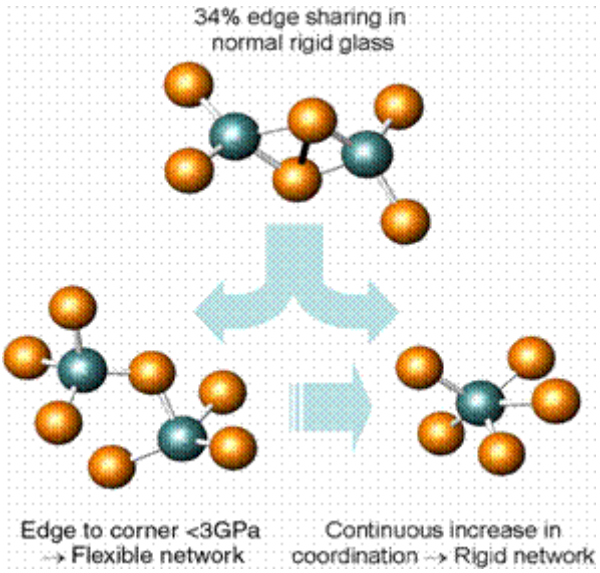

Fig. 3.5.2 Schematic diagrams showing the pathways of shear rigidity change when GeSe2 coordination network changes at different pressure range.

The minimum observed in the shear-wave velocity, associated anomalous behavior in Poisson's ratio, and discontinuities in elastic moduli at 4 GPa are indicative of a gradual structural transition in the glass. This is attributed to a network rigidity minimum originating from a competition between two densification mechanisms. At pressures up to 3 GPa, a conversion from edge- to corner- sharing tetrahedra results in a more flexible network. This is contrasted by a gradual increase in coordination number with pressure, which leads to an overall stiffening of the glass (Fig. 3.5.2). Since the From the measured sound velocities, we have obtained the density at high pressures, and the recovered sample has a permanent densification of 8%. This work opens new opportunities for the study of a wide range of materials, such as melts of crystalline materials and polymers which will be of great interest to the stewardship stockpile project.

4. Publications and Presentations

Journal Publications

1. Antao et al., PRL, S.M. Antao, C.J. Benmore, B.S. Li, L.P. Wang, E. Bychkov, J.B. Parise, Network rigidity in GeSe2 glass at high pressure, ***Phys. Rev. Lett***. 100, (2008)
2. Wei Liu, Baosheng Li, Liping Wang, Jianzhong Zhang, and Yusheng Zhao, Elasticity of ω-phase zirconium, ***Phys. Rev. B* 76**, 144107 (2007).
3. Matthew Whitaker, Wei Liu, Qiong Liu, Liping Wang, Baosheng Li, In-situ Compressional and Shear Wave Velocities Measurements on ε-FeSi, ***High Pressure Research***, in Material Under Extreme Coditions, Eds: Y. Wang and T., Irifune, 2008 (in press).
4. Jianzhong. Zhang, Baosheng Li, Y. Zhao, Donald Weidner, Pressure-induced shear-mode elastic softening in orthorhombic $BaCe_{0.85}Y_{0.15}O_{2.925}$ perovskite, ***High Pressure Research***, in Material Under Extreme Coditions, Eds: Y. Wang and T., Irifune, 2008 (in press).
5. Wei Liu, Baosheng Li, Liping Wang, Jianzhong Zhang, and Yusheng Zhao, Elasticity across the α–ω phase transition of zirconium, ***J, App. Phys***., 2008, (submitted)
6. Qiong Liu, Wei Liu, Matthew Whitaker, Baosheng Li, Sound velocity measurements on tantalum to 12 GPa, (to be submitted to ***Solid State Comm.***).

7 Baosheng Li, Wei Liu, Qiong Liu Liping Wang, Ultrasonic measurements of Sound Velocities across the γ–α phase transition in Cerium, ***App Phy Lett.***, 2008 (to be submitted).

8. Wei Liu, Qiong Liu, Matthew Whitaker, Baosheng Li, Simultaneous ultrasonic and X-ray Measurements on Molybdenum to 12 GPa 1273K, ***Phy Rev B***, (in preparation).
9. Wei Liu, Baosheng Li, Velocity and Density of ZrW2O8 glass at high pressure, ***Phy Rev B***., 2008 (in preparation).

Invited and Contributed Presentations/Conference Papers

1. Baosheng Li, Probing Material Properties at High Pressure and Temperature Using Phonons and Photons, Gordon Research Conference on High Pressure Research, Biddeford, UNE, June 29-July 4, 2008**(Invited)**.
2. Baosheng Li, Simultaneous Ultrasonic and X-ray Diffraction Measurements at High Pressure and High Temperature, Workshop on High Pressure Research, Beijing University, June 19-21, Beijing, China (**Invited**).
3. Baosheng Li, Thermoelasticity of SSP Materials, DoE/SSNA Workshop, February 6-8, Washington DC, 2008.
4. Qiong Liu, Matthew Whitaker, Wei Liu, Donald Isaak, Thermoelasticity Measurements at High Pressure and High Temperature, DoE/SSNA Workshop, February 6-8, Washington DC, 2008.
5. Matthew Whitaker, Wei Liu, Qiong Liu, Liping Wang Baosheng Li, In-situ Compressional and Shear Wave Velocities Measurements on ε-FeSi, COMPRES annual meeting, Colorado Spring, Colorado, June 25-28, 2008.
6. Matthew Whitaker, Wei Liu, Qiong Liu, Liping Wang Baosheng Li, Combined Ultrasonic and X-ray Measurements on ε-FeSi, International Workshop on High Pressure Research of New Materials, Advanced Photon Source, University of Chicago, Dec 3-5, 2007.

7. Jianzhong. Zhang, Baosheng Li, Y. Zhao, Donald Weidner, Pressure-induced shear-mode elastic softening in orthorhombic $BaCe_{0.85}Y_{0.15}O_{2.925}$ perovskite, International Workshop on High Pressure Research of New Materials, Advanced Photon Source, University of Chicago, Dec 3-5, 2007.
8. Wei Liu, Baosheng Li, Jiangzhong Zhang and Yusheng Zhao Simultaneous Ultrasonic and Synchrotron X-ray Studies on α and ω Phases of Zirconium at High Pressure, April 2007, CeSEMAC meeting, Florida International University, April, 2007 **(invited).**

5. References

[1] P. Soderlind, J.A. Moriarty, First-principles theory of Ta up to 10 Mbar pressure: Structural and mechanical properties, Phys. Rev. B 57(1998) 10340-10350.

[2] A. Schiwek, F. Porsch, W.B. Holzapfel, High temperature-high pressure structural studies of cerium, High Pressure Res 22(2002) 407-410.

[3] O. Gulseren, R.E. Cohen, High-pressure thermoelasticity of body-centered-cubic tantalum, Phys. Rev. B 65(2002).

[4] K.W. Katahara, M.H. Manghnani, E.S. Fisher, PRESSURE DERIVATIVES OF ELASTIC-MODULI OF NIOBIUM AND TANTALUM, J. Appl. Phys. 47(1976) 434-439.

[5] A. Dewaele, P. Loubeyre, Mechanical properties of tantalum under high pressure, Phys. Rev. B 72(2005) 9.

[6] D. Orlikowski, P. Soderlind, J.A. Moriarty, First-principles thermoelasticity of transition metals at high pressure: Tantalum prototype in the quasiharmonic limit, Phys. Rev. B 74(2006) 10.

[7] Z.L. Liu, L.C. Cai, X.R. Chen, F.Q. Jing, Molecular dynamics simulations of the melting curve of tantalum under pressure, Phys. Rev. B 77(2008) 9.

[8] S.N. Luo, D.C. Swift, On high-pressure melting of tantalum, Physica B 388(2007) 139-144.

[9] W.J. Nellis, A.C. Mitchell, D.A. Young, Equation-of-state measurements for aluminum, copper, and tantalum in the pressure range 80-440 GPa, (0.8-4.4 Mbar), J. Appl. Phys. 93(2003) 304-310.

[10] D. Errandonea, M. Somayazulu, D. Hausermann, H.K. Mao, Melting of tantalum at high pressure determined by angle dispersive x-ray diffraction in a double-sided laser-heated diamond-anvil cell, J. Phys.-Condes. Matter 15(2003) 7635-7649.

[11] H. Chikh, A. Afir, A. Pialoux, High temperature X-ray diffraction study of tantalum behaviour under vacuum or under controlled carbon monoxide pressure, Ann. Chim.-Sci. Mat. 31(2006) 621-630.

[12] O. Gulseren, R.E. Cohen, High-pressure thermoelasticity of body-centered-cubic tantalum, Phys. Rev. B 65(2002) 5.

[13] M. Hanfland, K. Syassen, J. Kohler, Pressure-volume relationship of Ta, J. Appl. Phys. 91(2002) 4143-4148.

[14] B. Li, J. Kung, R.C. Liebermann, Modern techniques in measuring elasticity of Earth materials at high pressure and high temperature using ultrasonic interferometry in conjunction with synchrotron X-radiation in multi-anvil apparatus, Phys. Earth Planet. Inter. 143-144(2004) 559-574.

[15] B.S. Li, K. Woody, J. Kung, Elasticity of MgO to 11 GPa with an independent absolute pressure scale: Implications for pressure calibration, J. Geophys. Res.-Solid Earth 111(2006) -.

[16] B.S. Li, J.Z. Zhang, Pressure and temperature dependence of elastic wave velocity of MgSiO3 perovskite and the composition of the lower, Phys. Earth Planet. Inter. 151(2005) 143-154.

[17] W. Liu, J. Kung, B.S. Li, Elasticity of San Carlos olivine to 8 GPa and 1073 K, Geophys. Res. Lett.

32(2005) -.

[18] J. Kung, B.S. Li, R.C. Liebermann, Ultrasonic observations of elasticity changes across phase transformations in MgSiO3 pyroxenes, J. Phys. Chem. Solids 67(2006) 2051-2055.

[19] J. Kung, B.S. Li, T. Uchida, Y.B. Wang, In-situ elasticity measurement for the unquenchable high-pressure clinopyroxene phase: Implication for the upper mantle, Geophys. Res. Lett. 32(2005) -.

[20] B.S. Li, J. Kung, R.C. Liebermann, Modem techniques in measuring elasticity of Earth materials at high pressure and high temperature using ultrasonic interferometry in conjunction with synchrotron X-radiation in multi-anvil apparatus, Physics of the Earth and Planetary Interiors 143-44(2004) 559-574.

[21] B.S. Li, K. Chen, J. Kung, R.C. Liebermann, D.J. Weidner, Sound velocity measurement using transfer function method, J. Phys.-Condes. Matter 14(2002) 11337-11342.

[22] H.M. J. Xu, and P. M. Bell,, High Temperatures-High Pressures 16(1984) 495.

[23] H. Cynn, C.S. Yoo, Equation of state of tantalum to 174 GPa, Phys. Rev. B 59(1999) 8526-8529.

[24] A. Dewaele, P. Loubeyre, M. Mezouar, Equations of state of six metals above 94 GPa, Phys. Rev. B 70(2004) 094112.

[25] J.C. Boettger, Equation of state for tantalum from relativistic linear combinations of Gaussian-type orbitals calculations, Phys. Rev. B 6403(2001).

[26] K.W. Katahara, M.H. Manghnani, E.S. Fisher, Pressure derivatives of the elastic moduli of niobium and tantalum, J. Appl. Phys. 47(1976) 434-439.

[27] O. Gülseren, R.E. Cohen, High-pressure thermoelasticity of body-centered-cubic tantalum, Phys. Rev. B 65(2002) 064103.

[28] L. Ming, M.H. Manghnani, ISOTHERMAL COMPRESSION OF BCC TRANSITION-METALS TO 100 KBAR, J. Appl. Phys. 49(1978) 208-212.

[29] E. Walker, and Bujard, P., Sol. State Comm 34, 691-693, 1980(1980) 691-693.

[30] N. Soga, Comparison of Measured and Predicted Bulk Moduli of Tantalum and Tungsten at High Temperatures, J. Appl. Phys. 37(1966) 3416-&.

[31] L. Stixrude, C. Lithgow-Bertelloni, Thermodynamics of mantle minerals - I. Physical properties, Geophys. J. Int. 162(2005) 610-632.

[32] Y.W. Fei, H. Li, K. Hirose, W. Minarik, J. Van Orman, C. Sanloup, W. van Westrenen, T. Komabayashi, K. Funakoshi, A critical evaluation of pressure scales at high temperatures by in situ X-ray diffraction measurements, Phys Earth Planet In 143-44(2004) 515-526.

[33] T.S. Duffy, T.J. Ahrens, Dynamic-Response of Molybdenum Shock-Compressed at 1400-Degrees-C, J Appl Phys 76(1994) 835-842.

[34] J.A. Moriarty, Ultrahigh-Pressure Structural Phase-Transitions in Cr, Mo, and W, Phys Rev B 45(1992) 2004-2014.

[35] A.M. Molodets, Shock compression of preheated molybdenum, High Pressure Res 25(2005) 211-216.

[36] K.W. Katahara, M.H. Manghnani, E.S. Fisher, Pressure Derivatives of the Elastic-Moduli of Bcc Ti-V-Cr, Nb-Mo and Ta-W Alloys, J Phys F Met Phys 9(1979) 773-790.

[37] Y.S. Zhao, A.C. Lawson, J.Z. Zhang, B.I. Bennett, R.B. Von Dreele, Thermoelastic equation of state of molybdenum, Phys. Rev. B 62(2000) 8766-8776.

[38] D.I. Bolef, J. Deklerk, Elastic Constants of Single-Crystal Mo and W between 77 Degrees and 500 Degrees K, J. Appl. Phys. 33(1962) 2311-&.

[39] F.H. Featherston, J.R. Neighbours, Elastic Constants of Tantalum, Tungsten, and Molybdenum, Phys Rev 130(1963) 1324-&.

[40] Dickinso.Jm, Armstron.Pe, Temperature Dependence of Elastic Constants of Molybdenum, J Appl Phys 38(1967) 602-&.

[41] D.L. Davidson, F.R. Brotzen, Elastic Properties of Molybdenum-Rhenium Alloys, Jom-J Min Met Mat S 20(1968) A83-&.

[42] Y.K. Vohra, A.L. Ruoff, Static Compression of Metals Mo, Pb, and Pt to 272 Gpa - Comparison with Shock Data, Phys. Rev. B 42(1990) 8651-8654.

[43] Y. Zhao, A.C. Lawson, J. Zhang, B.I. Bennett, R.B. Von Dreele, Thermoelastic equation of state of molybdenum, Phys. Rev. B 62(2000) 8766.

[44] I.K. Jeong, T.W. Darling, M.J. Graf, T. Proffen, R.H. Heffner, Y. Lee, T. Vogt, J.D. Jorgensen, Role of the lattice in the gamma ->alpha phase transition of Ce: A high-pressure neutron and X-ray diffraction study, Phys Rev Lett 92(2004) -.

[45] Y.K. Vohra, S.L. Beaver, J. Akella, C.A. Ruddle, S.T. Weir, Ultrapressure equation of state of cerium metal to 208 GPa, J Appl Phys 85(1999) 2451-2453.

[46] Y. Zhao, W.B. Holzapfel, Structural studies on the phase diagram of cerium, J Alloy Compd 246(1997) 216-219.

[47] G.L. Gu, Y.K. Vohra, K.E. Brister, Crystal Grain-Growth during Phase-Transformation in Cerium Metal at High-Pressure, Phys Rev B 52(1995) 9107-9110.

[48] P. Soderlind, O. Eriksson, J. Trygg, B. Johansson, J.M. Wills, Density-Functional Calculations for Cerium Metal, Phys Rev B 51(1995) 4618-4621.

[49] M.I. McMahon, R.J. Nelmes, Different results for the equilibrium phases of cerium above 5 GPa, Phys Rev Lett 78(1997) 3884-3887.

[50] P. Ravindran, L. Nordstrom, R. Ahuja, J.M. Wills, B. Johansson, O. Eriksson, Theoretical investigation of the high-pressure phases of Ce, Phys Rev B 57(1998) 2091-2101.

[51] G. Eliashberg, H. Capellmann, On the nature of the gamma-alpha phase transition in cerium, Jetp Lett+ 67(1998) 125-132.

[52] S.M. Antao, C.J. Benmore, B.S. Li, L.P. Wang, E. Bychkov, J.B. Parise, Network rigidity in GeSe2 glass at high pressure, Phys. Rev. Lett. 100(2008) -.

[53] Q. Mei, C.J. Benmore, R.T. Hart, E. Bychkov, P.S. Salmon, C.D. Martin, F.M. Michel, S.M. Antao, P.J. Chupas, P.L. Lee, S.D. Shastri, J.B. Parise, K. Leinenweber, S. Amin, J.L. Yarger, Topological changes in glassy GeSe2 at pressures up to 9.3 GPa determined by high-energy x-ray and neutron diffraction measurements, Phys. Rev. B 74(2006) -.